IEEE Access
Multidisciplinary | Rapid Review | Open Access Journal

Received 14 June 2023, accepted 11 July 2023, date of publication 14 July 2023, date of current version 21 July 2023.

Digital Object Identifier 10.1109/ACCESS.2023.3295692

RESEARCH ARTICLE

A Quantitative Microwave Imaging Approach for Brain Stroke Classification Based on the Generalized Tikhonov Regularization

SAYYED SALEH SAYYED MOUSAVI[1] AND MOHAMMAD SAEED MAJEDI[2]
[1]Communications and Computer Research Center, Ferdowsi University of Mashhad, Mashhad 9177948883, Iran
[2]Department of Electrical Engineering, Ferdowsi University of Mashhad, Mashhad 9177948883, Iran

Corresponding author: Mohammad Saeed Majedi (majedi@um.ac.ir)

ABSTRACT Early diagnosis of stroke type by imaging is one of the most important tasks for stroke patients. In this article, we propose a new approach to reconstruct the brain image with high accuracy and quality. In this approach, first we use the Born iterative method to reconstruct the brain image. Then by comparing this image with a set of MRI-based brain images, using structural similarity index measure criterion, we choose the best one as reference image. Finally, we reconstruct the brain image by distorted Born iterative method or Born iterative method along with generalized Tikhonov regularization using the reference image. The reconstructed images are compared with those that obtained based on Tikhonov regularization. These comparisons demonstrate that the accuracy and quality of images in the proposed approach are significantly increased.

INDEX TERMS Microwave imaging, generalized Tikhonov regularization, brain stroke classification.

I. INTRODUCTION

One of the main causes of death and disability worldwide is brain stroke [1], [2]. It can be divided into hemorrhagic stroke, which is bleeding in the brain, and ischemic stroke, in which blood flow is limited by a blood clot. The majority of stroke cases–about 80%–are ischemic and about 20% of them are hemorrhagic. Within 3–4.5 hours following the onset of stroke symptoms, the clinical choice to provide a proper action should be made [1], and it is based on imaging techniques like computed tomography (CT) and magnetic resonance imaging (MRI) [2].

Due to a number of benefits over more traditional imaging modalities like CT or MRI, microwave imaging (MWI) is a method that has recently gained growing interest. It offers a non-intrusive evaluation of the structural and functional state of biological tissues. It uses nonionizing radiation in the low (GHz) part of the electromagnetic spectrum and hence the patient is safe. Additionally, the technology may be made small and portable, making it possible to use MWI technology in mobile applications. The usability and comparatively inexpensive price are further benefits. MWI is only constrained by the amount of time required for image reconstruction because the data acquisition time of an MWI device is in the range of milliseconds to a few seconds. Finally unlike MRI, it is a silent technology and suitable for people who are claustrophobic. The relatively weak spatial resolution, which is related to the frequency spectrum used, is a disadvantage. Due to the substantial attenuation of the brain tissues, this frequency spectrum is particularly constrained for applications involving brain imaging. However, MWI, a novel imaging modality, can be a useful method addition to already well-recognized imaging technologies, like the aforementioned CT or MRI [1], [3].

Recently, many researches for reconstruction of brain images and detection of tumor and stroke using microwave imaging have been done [4], [5]. For example, in [2] for brain stroke detection and monitoring, a helmet with 177 waveguide antennas has been fabricated. Reconstructed images using finite difference time domain and finite element methods were related to a 3D simple phantom. In this article the hemorrhagic stroke is well observed however the detection of the ischemic stroke is difficult. In [8], to reconstruct the brain images quickly, the computational

The associate editor coordinating the review of this manuscript and approving it for publication was Roberta Palmeri.

domain has been divided into several sections for parallel computation and a high-performance computing machine has been applied. Although the reconstructed time for 3D brain phantom reduced to 94 seconds from 2 hours, the quality of the reconstructed images was low. In [6], a combination of the contrast source inversion method and the finite element method has been proposed to reconstruct the head images. The authors have presented a novel approach for discretizing contrast sources that simplifies the algorithm implementation and improves the accuracy of computed quantities. In [7], the authors have implemented a non-linear microwave imaging approach using DBIM with GPU-accelerated FDTD and compare 2-D and 3-D microwave tomography implementations for head imaging and stroke detection in a numerical head phantom.

The inverse scattering problems are ill-posed, hence the regularization method should be used. Applying a proper regularization method can improve the quality of images.

Reference [9] introduces a new regularization algorithm based on the Newton-Conjugate-Gradient Method in L^p Banach Spaces for brain imaging. This algorithm improves the convergence properties and the accuracy of reconstructed images, however it needs to a prior information. In [10], the inverse scattering problem is solved in a variable exponent Lebesgue space $L^{p(\cdot)}$ $(1 < p < 2)$ for brain images. In this article a mechanism to determine the value of p according to the pixel location of the corresponding image (inside the brain or outside of it) is introduced and the reconstruction of brain image with hemorrhagic stroke is done. In [11], Winters et al. utilize both ℓ_1 and ℓ_2 penalties to regularize the system of linear equations in each iteration of the distorted Born iterative method (DBIM). The effect of the ℓ_2 penalty is to stabilize the results while ℓ_1 is used for sparsity. In [12], a comparison of an enhanced DBIM and the multiplicative-regularized (MR) contrast source inversion (CSI) method is done. In the enhanced DBIM, two different regularizations, multiplicative and laplacian regularizations, are utilized. The result of this comparison shows that the result of these regularization methods are the same however the implementation and computational complexity of MR-CSI is better than those of enhanced DBIM. In [13] and [14], a new regularization term is introduced for DBIM which is related to the induced current instead of contrast. Using this regularization term in [13] leads to more robustness against noise compared to DBIM with Tikhonov regularization. In [14], using an approximation in the regularization term of [13], leads to reduction of computation burden in the 3D inverse scattering problems. In [15] a new integral equation (NIE) is proposed to tackle the severe ill-posedness and strong nonlinearity in inverse scattering problems. In [16] a hybrid regularization technique is utilized to solve this NIE. Using this proposed method, the image of strong scatterer can be reconstructed. In [17],the authors propose a fast 3D algorithm for solving the inverse scattering problem that does not need the regularization method. In this algorithm a smooth basis function is used which reduces the number of variables for mapping the permittivity.

The tissue of brain is complex. Hence in the problem of reconstructing its image for high accuracy stroke classification, it is necessary to use a proper method that can reconstruct such complex medium. In this paper, we propose a new approach for solving the inverse scattering problem based on the generalized Tikhonov regularization in conjunction with BIM and DBIM. This approach leads to high quality brain images reconstruction for stroke classification. In this approach, first we use BIM with Tikhonove regularization to reconstruct brain images from scattering data. Then we compare it with a set of MRI-based brain images in order to choose a suitable reference image. Finally we reconstruct the brain image using BIM or DBIM with generalized Tikhonov regularization based on this reference image.

The proposed approach has two contributions. First application of the generalized Tikhonov regularization method in brain microwave imaging, and second, the selection procedure of the reference image for the generalized Tikhonov regularization operator.

This paper is organized as follows. In the second section, we introduce the electromagnetic scattering problem. Tikhonov regularization method for solving the ill-posed problem and two quantitatively method, BIM and DBIM, are described in this section. In the third section, we introduce our proposed approach that utilizes a special type of generalized Tikhonov regularization in BIM and DBIM in order to reconstruct the high quality images. In the fourth section we present numerical results and compare the reconstructed images with those of obtained by BIM and DBIM with Tikhonov regularization.

II. ELECTROMAGNETIC SCATTERING

In the scattering theory, we have the Lippmann-Schwinger integral equation in 2D medium [18] as follows

$$E^{tot}(r) = E^{inc}(r) - \omega^2 \mu \varepsilon_0 \int_{D_i} G_b(r, r') \chi(r') E^{tot}(r') dr' \quad (1)$$

In (1), the second term on the right is the scattered field and is composed of an integral over the investigation domain D_i. $G_b(r, r')$ is the background Green's function (i.e. Green's function of the domain without the scatterers). $\chi(r) = \varepsilon_r(r) - \varepsilon_r^b$ is the contrast function that is the difference between the investigation domain and background relative permittivities. $E^{tot}(r)$ is the total field (i.e. the electric field in the medium with scatterers) and $E^{inc}(r)$ is the incident field in the background medium.

Equation (1) can be written in two different media. The first medium is the investigation domain, and the second one is the measurement domain, which is the medium composed of observation points. The equation written in the investigated domain $r \in D_i$ is the state equation (2), and the equation written in the measurement domain $r \in D_m$ is the data equation (3).

$$E^{tot}(r) = E^{inc}(r) - \omega^2 \mu \varepsilon_0 \int_{D_i} G_D(r, r') \chi(r') E^{tot}(r') dr' \quad (2)$$

$$E^{scat}(r) = -\omega^2 \mu \varepsilon_0 \int_{D_i} G_s(r, r')\chi(r')E^{tot}(r')dr' \tag{3}$$

$G_D(r, r')$ and $G_s(r, r')$ are the Green's functions from the investigation domain to the investigation domain and the measurement domain, respectively.

In forward scattering problem, first we calculate the total field from (2) and then apply it in (3) to acquire the scattering fields from an object. The inverse scattering problem is intrinsically non-linear and ill-posed. Non-linearity can be resolved using iterative methods, however to resolve the ill-posedness of the problem, it is necessary to utilize regularization methods. In the next subsections, we present the Tikhonov and generalized Tikhonov regularization methods and then the BIM and DBIM using Tikhonov regularization.

A. TIKHONOV AND GENERALIZAD TIKHONOV REGULARIZATION METHODS

Tikhonov regularization is the most commonly used method for regularizing ill-posed problems [18]. If the matrix equation $\bar{\bar{A}}\bar{x} = \bar{b}$ is an ill-posed problem, in the Tikhonov regularization, we should solve the following optimization problem

$$\underset{x}{Min} \left\| \bar{\bar{A}}\bar{x} - \bar{b} \right\|^2 + \lambda \|\bar{x}\|^2 \tag{4}$$

In the (4), λ is the regularization parameter and can be determined by several methods such as L-Curve or Generalized Cross Validation methods [18]. The closed form of the solution of (4) is

$$\bar{x} = \left(\bar{\bar{A}}^H \bar{\bar{A}} + \lambda \bar{\bar{I}} \right)^{-1} \bar{\bar{A}}^H \bar{b} \tag{5}$$

In generalized Tikhonov regularization method, we should solve the following optimization problem

$$\underset{x}{Min} \left\| \bar{\bar{A}}\bar{x} - \bar{b} \right\|^2 + \lambda \left\| \bar{\bar{L}}\bar{x} \right\|^2 \tag{6}$$

In (6), L is a regularization operator. The closed form of the solution of (6) is

$$x = \left(\bar{\bar{A}}^H \bar{\bar{A}} - \lambda \bar{\bar{L}}^H \bar{\bar{L}} \right)^{-1} \bar{\bar{A}}^H \bar{b} \tag{7}$$

B. BORN ITERATIVE METHOD

BIM is an iterative method that utilizes the Born approximation at each iteration [19]. At the kth iteration of this method, first the total field $E^{tot}_{k-1}(r)$ is computed for the contrast function obtained in the previous iteration, $\chi_{k-1}(r)$, using the state equation (2). Then by substituting $E^{tot}_{k-1}(r)$ in the data equation (3) and using a regularization method, the inverse problem is solved to achieve $\chi_k(r)$. For the first iteration, $\chi_0(r)$ is chosen arbitrarily.

Matrix form of (2) and (3) are as follows, respectively

$$\bar{E}^{tot}_{k-1} = \bar{E}^{inc} + \bar{\bar{G}}_D \cdot \bar{\bar{\chi}}_{k-1} \cdot \bar{E}^{tot}_{k-1} \tag{8}$$

$$\bar{E}^{scat} = \bar{\bar{G}}_s \cdot \bar{\bar{\chi}}_k \cdot \bar{E}^{tot}_{k-1} \tag{9}$$

For solving (9) using Tikhonov regularization method, the following optimization problem should be solved

$$\underset{\bar{\bar{\chi}}}{Min} \sum_{i=1}^{N_i} \left\| \bar{E}^{scat,i} - \bar{\bar{G}}_s \cdot \bar{\bar{\chi}} \cdot \bar{E}^{tot,i}_{k-1} \right\|^2 + \lambda \left\| \bar{\bar{\chi}} \right\|^2 \tag{10}$$

in which N_i is the number of transmitters. The closed form of the solution of (10) is as follows

$$\bar{\bar{\chi}} = \left(\left(\sum_{i=1}^{N_i} \bar{\bar{G}}_s \cdot \bar{E}^{tot,i}_{k-1} \right)^H \cdot \left(\sum_{i=1}^{N_i} \bar{\bar{G}}_s \cdot \bar{E}^{tot,i}_{k-1} \right) + \lambda \bar{\bar{I}} \right)^{-1} \cdot \left(\left(\sum_{i=1}^{N_i} \bar{\bar{G}}_s \cdot \bar{E}^{tot,i}_{k-1} \right)^H \cdot \left(\sum_{i=1}^{N_i} \bar{E}^{scat,i} \right) \right) \tag{11}$$

C. DISTORTED BORN ITERATIVE METHOD

DBIM is an iterative method that is similar to BIM, except that in DBIM the the effective inhomogeneous background Green's function is used that is updated at each iteration [20]. In this method, at the kth iteration, the difference of the contrast functions at the current and previous iteration $\delta\chi_{k-1} = \chi_k - \chi_{k-1}$ is reconstructed. The state equation in DBIM is the same as the BIM but the data equation is as follows

$$E^{scat}(r) = -\omega^2 \mu \varepsilon_0 \int_{D_i} G_s(r, r')\chi_{k-1}(r')E^{tot}_{k-1}(r')dr' - \omega^2 \mu \varepsilon_0 \int_{D_i} G^{bs}_{k-1}(r, r')\delta\chi_{k-1}(r')E^{tot}_{k-1}(r')dr' \tag{12}$$

In (12), the first term on the right is the scattered field caused by χ_{k-1} and the second term is the scattered field caused by $\delta\chi_{k-1}$ in which the background medium is related to χ_{k-1}. The matrix form of the data equation (12) is as follow

$$\bar{E}^{scat} = \bar{\bar{G}}_s \cdot \bar{\bar{\chi}}_{k-1} \cdot \bar{E}^{tot}_{k-1} + \bar{\bar{G}}^{bs}_{k-1} \cdot \delta\bar{\bar{\chi}}_{k-1} \cdot \bar{E}^{tot}_{k-1} \tag{13}$$

In (13), the inhomogeneous background Green's function $\bar{\bar{G}}^{bs}_{k-1}$ and the total field calculated for $\bar{\bar{\chi}}_{k-1}$, $\bar{E}^{tot}_{k-1}$, are as follows [13], [18]

$$\bar{\bar{G}}^{bs}_{k-1} = \bar{\bar{G}}_s \cdot \left(\bar{\bar{I}} - \bar{\bar{\chi}}_{k-1} \cdot \bar{\bar{G}}_D \right)^{-1} \tag{14}$$

$$\bar{E}^{tot}_{k-1} = \left(\bar{\bar{I}} - \bar{\bar{\chi}}_{k-1} \cdot \bar{\bar{G}}_D \right)^{-1} \cdot \bar{E}^{inc} \tag{15}$$

For solving (13) using Tikhonov regularization method, the following optimization problem should be solved

$$\underset{\delta\bar{\bar{\chi}}}{Min} \sum_{i=1}^{N_i} \left\| \begin{matrix} \bar{E}^{scat}_i - \bar{\bar{G}}_s \cdot \bar{\bar{\chi}}_{k-1} \cdot \bar{E}^{tot,i}_{k-1} \\ -\bar{\bar{G}}^{bs}_{k-1} \cdot \delta\bar{\bar{\chi}} \cdot \bar{E}^{tot,i}_{k-1} \end{matrix} \right\|^2 + \lambda \left\| \delta\bar{\bar{\chi}} \right\|^2 \tag{16}$$

and the closed form of the solution of (16) is as follows

$$\delta\bar{\bar{\chi}} = \left(\left(\sum_{i=1}^{N_i} \bar{\bar{G}}^{bs}_{k-1} \cdot \bar{E}^{tot,i}_{k-1} \right)^H \cdot \left(\sum_{i=1}^{N_i} \bar{\bar{G}}^{bs}_{k-1} \cdot \bar{E}^{tot,i}_{k-1} \right) + \lambda \bar{\bar{I}} \right)^{-1}$$

$$\cdot\left(\sum_{i=1}^{N_i}\bar{\bar{G}}_{k-1}^{bs}\cdot\bar{E}_{k-1}^{tot,i}\right)^{H}$$
$$\cdot\left(\sum_{i=1}^{N_i}\bar{E}^{scat,i}-\bar{\bar{G}}_s\cdot\bar{\bar{\chi}}_{k-1}\cdot\bar{E}_{k-1}^{tot,i}\right) \quad (17)$$

III. PROPOSED APPROACH

Our proposed approach is composed of three steps: first, we reconstruct the brain image by the BIM with Tikhonov regularization method. Then this image is compared with a set of MRI-based brain images using the structural similarity index measure (SSIM) [21] criterion in order to choose a most similar image to the original profile as reference image. Finally, we use the BIM or DBIM with the generalized Tikhonov regularizaion and reference image in order to reconstruct the brain images. Fig. 1 shows the flowchart of the proposed approach.

In the generalizad Tikhonov regularization for BIM, we utilize the regularization operator as follow

$$L = x - x^r \quad (18)$$

that x^r is the reference image. Hence for solving (9) by the regularization operator (18), we should solve the following optimization problem

$$\underset{\chi}{Min}\sum_{i=1}^{N_i}\left\|\bar{E}^{scat,i}-\bar{\bar{G}}_s\cdot\bar{\bar{\chi}}\cdot\bar{E}_{k-1}^{tot,i}\right\|^2+\lambda\left\|\bar{\bar{\chi}}-\bar{\bar{\chi}}^r\right\|^2 \quad (19)$$

and the closed form of the solution of (19) is

$$\chi=\left(\left(\sum_{i=1}^{N_i}\bar{\bar{G}}_s\cdot\bar{E}_{k-1}^{tot,i}\right)^{H}\cdot\left(\sum_{i=1}^{N_i}\bar{\bar{G}}_s\cdot\bar{E}_{k-1}^{tot,i}\right)+\lambda\bar{\bar{I}}\right)^{-1}$$
$$\cdot\left(\left(\sum_{i=1}^{N_i}\bar{\bar{G}}_s\cdot\bar{E}_{k-1}^{tot,i}\right)^{H}\cdot\left(\sum_{i=1}^{N_i}\bar{E}^{scat,i}\right)+\lambda\bar{\bar{\chi}}^r\right) \quad (20)$$

In the generalizad Tikhonov regularization for DBIM, we utilize the regularization operator as follow

$$L = x - x^p \quad (21)$$

in which $x^p = mx^r$. Hence the solution of (13) using the regularization operator (21), can be obtained by solving the following optimization problem

$$\underset{\delta\bar{\bar{\chi}}}{Min}\sum_{i=1}^{N_i}\left\|\begin{matrix}\bar{E}_i^{scat}-\bar{\bar{G}}_s\cdot\bar{\bar{\chi}}_{k-1}\cdot\bar{E}_{k-1}^{tot,i}\\-\bar{\bar{G}}_{k-1}^{bs}\cdot\delta\bar{\bar{\chi}}\cdot\bar{E}_{k-1}^{tot,i}\end{matrix}\right\|^2+\lambda\left\|\delta\bar{\bar{\chi}}-mx^r\right\|^2 \quad (22)$$

and the closed form of the solution of (22) is as follows

$$\delta\chi$$
$$=\left(\left(\sum_{i=1}^{N_i}\bar{\bar{G}}_{k-1}^{bs}\cdot\bar{E}_{k-1}^{tot,i}\right)^{H}\cdot\left(\sum_{i=1}^{N_i}\bar{\bar{G}}_{k-1}^{bs}\cdot\bar{E}_{k-1}^{tot,i}\right)+\lambda\bar{\bar{I}}\right)^{-1}$$

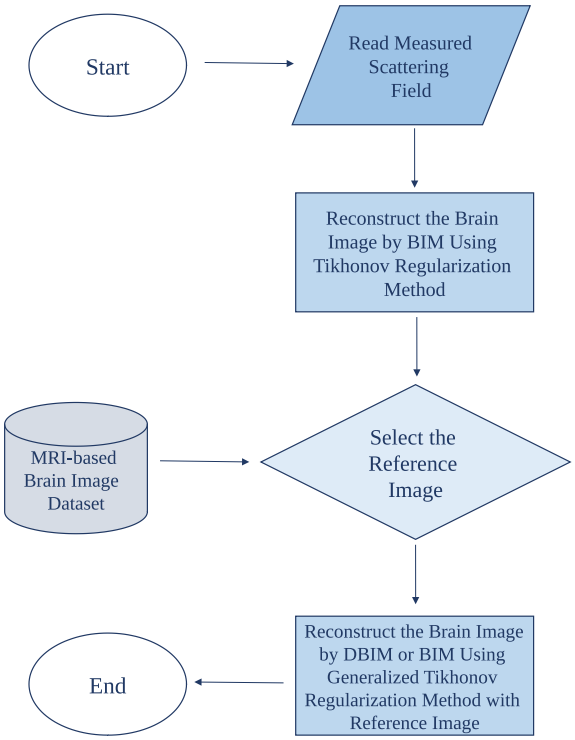

FIGURE 1. The flowchart of the proposed approach.

$$\cdot\left(\sum_{i=1}^{N_i}\bar{\bar{G}}_{k-1}^{bs}\cdot\bar{E}_{k-1}^{tot,i}\right)^{H}$$
$$\cdot\left(\left(\sum_{i=1}^{N_i}\bar{E}^{scat,i}-\bar{\bar{G}}_s\cdot\bar{\bar{\chi}}_{k-1}\cdot\bar{E}_{k-1}^{tot,i}\right)+\lambda mx^r\right) \quad (23)$$

In (22), if m is small, this regularization is similar to Tikhonov one and if m is large, this approach can not reconstruct the brain image. The best value for m is a number near to zero and can be obtained with trail and error.

IV. RESULTS AND DISCUSSION

In this section, we reconstruct the 2D brain images with stroke at 0.85 GHz using the proposed approach. The object is a brain phantom from "BrainWeb" database [22], [23] obtained from realistic 3D MRI images of 20 healthy person. Each 3D images consist of 362 two-dimensional images. Each pixel of these images is related to a specific tissue. We replace the value of pixels with relative permittivity and conductivity coefficients at 0.85 GHz [24]. The investigation domain is a square with a side length of 0.2 m and is composed of 1600 pixels. The head phantom which is embedded in a lossless matching medium with relative permittivity 44, is indefinitely long and non-magnetic. The frequency of solving the scattering problem is 0.85 GHz and the object is illuminated by TM fields. Transmitters are 24 line sources that located on a circle with a radius of 0.1 m. The number of observation points are 24 and located exactly on 24 transmitters.

We choose the section 220 from the phantom number 04 as the object. For modeling the hemorrhagic stroke, we use the

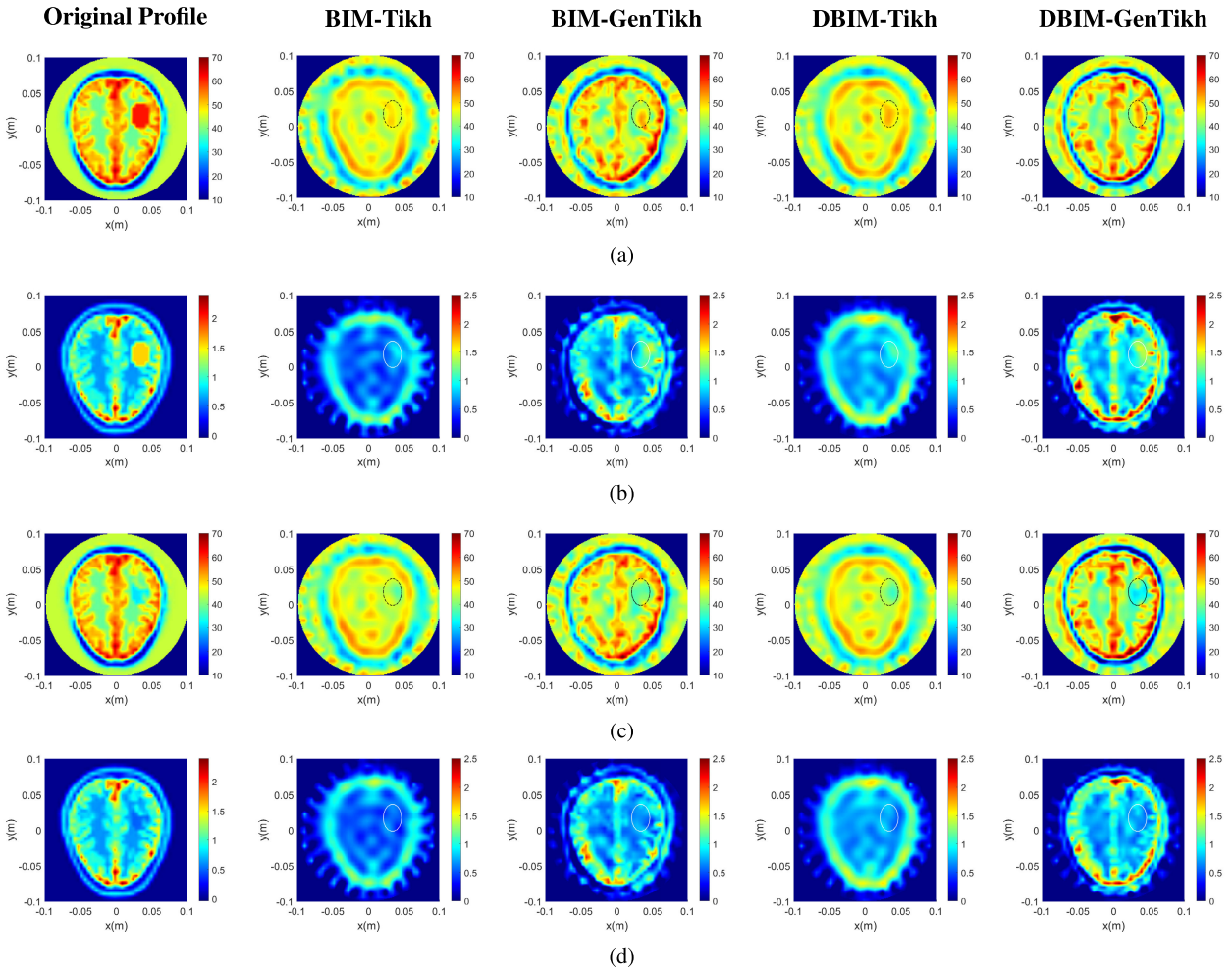

FIGURE 2. Reconstruction of brain images with four different methods and SNR = 30dB for section 220 from phantom number 04. The first column is the original profile, the second column is images obtained by BIM with the Tikhonov regularization method, the third column is images obtained by BIM with the generalized Tikhonov regularization method, the forth column is images obtained by DBIM with the Tikhonov regularization method, and the fifth column is images obtained by DBIM with the generalized Tikhonov regularization method. (a) and (b) are relative permittivity and conductivity for hemorrhagic stroke, respectively. (c) and (d) are relative permittivity and conductivity for ischemic stroke, respectively.

relative permittivity and conductivity of blood at frequency 0.85 GHz. The ischemic stroke is modeled by a medium that its relative permittivity and conductivity are 20% less than those of healthy brain tissue.

The scattering fields, which obtained numerically by Moment Method, are summed with white Gaussian noise. The average of this noise is zero and its standard deviation σ is obtained from the following relationship according to the desired SNR value

$$SNR = 10\log_{10}\frac{\left\|E^{scat}\right\|^2}{2N_iN_r\sigma^2} \tag{24}$$

N_i and N_r are the number of transmitters and observation points, respectively.

The reference image for generalized Tikhonov is selected from a dataset composed of MRI images of 15 different heads which are obtained from BrainWeb database. These images are corresponding to phantom numbers 38, 41, 42, 43, 44, 45, 46, 47, 48, 49, 50, 51, 52, 53, and 54.

TABLE 1. The SSIM and NRMSE for reconstructed images of phantom number 04 section 220 with hemorrhagic stroke and 30dB SNR.

Methods	SSIM		NRMSE	
	permittivity	conductivity	permittivity	conductivity
BIM-Tikh	0.3892	0.3263	0.1756	0.4501
BIM-GenTikh	0.5247	0.4222	0.1414	0.3630
DBIM-Tikh	0.4049	0.3427	0.1580	0.3808
DBIM-GenTikh	0.5256	0.4510	0.1324	0.3510

In Figs. 2 and 3, the reconstructed images are depicted with two different SNR levels of 30dB and 20dB, respectively. The first column is the original profile and the second to fourth columns represents the brain images obtained by BIM with Tikhonov regularization (BIM-Tikh), BIM with generalized Tikhonov regularization (BIM-GenTikh), DBIM with Tikhonov regularization (DBIM-Tikh) and DBIM with generalized Tikhonov regularization (DBIM-GenTikh), respectively. The number of iteration in all of these methods is ten.

For both relative permittivity and conductivity images, two comparison criteria, SSIM and normalized root mean square

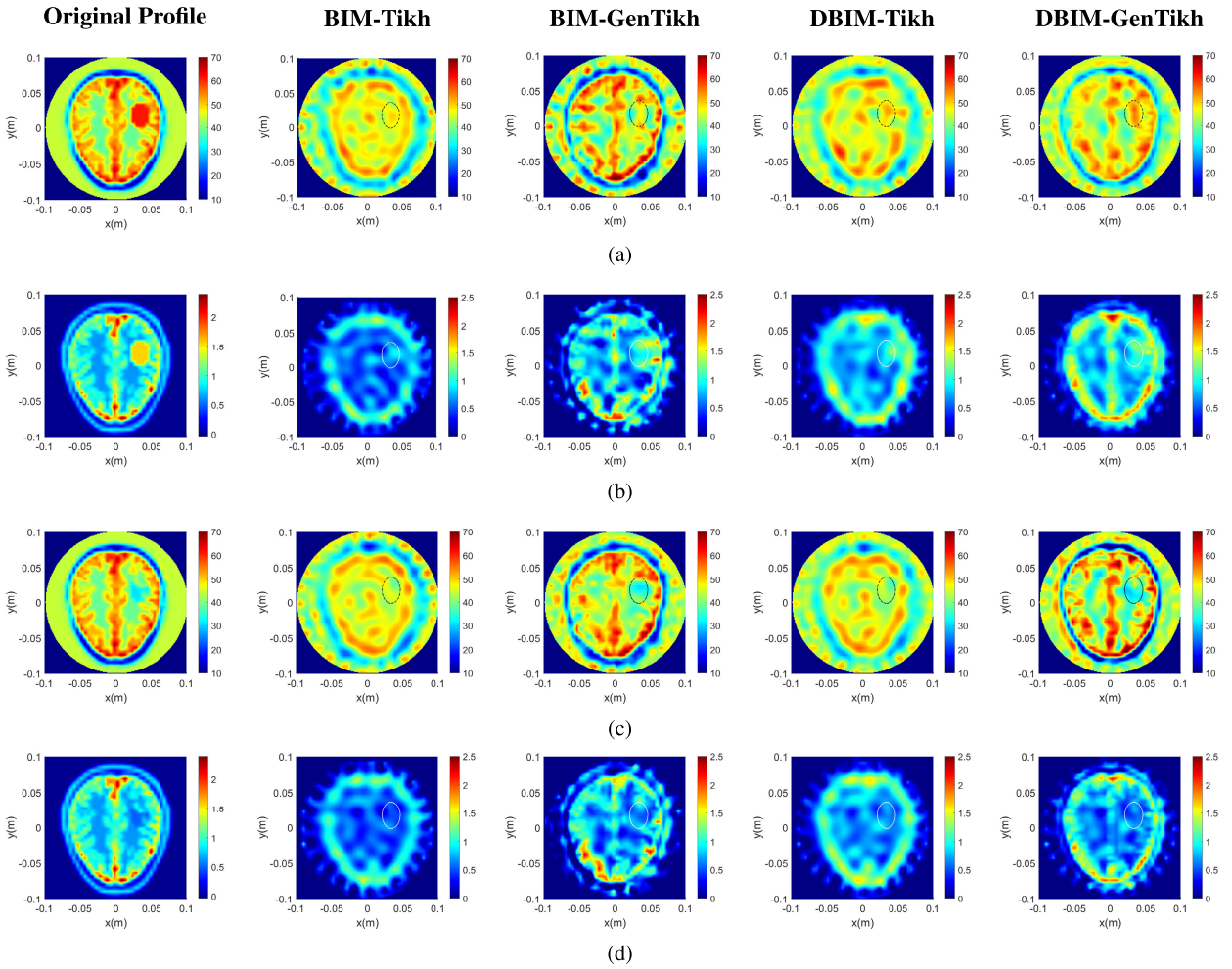

FIGURE 3. Reconstruction of brain images with four different methods and SNR = 20dB for section 220 from phantom number 04. The first column is the original profile, the second column is images obtained by BIM with the Tikhonov regularization method, the third column is images obtained by BIM with the generalized Tikhonov regularization method, the forth column is images obtained by DBIM with the Tikhonov regularization method, and the fifth column is images obtained by DBIM with the generalized Tikhonov regularization method. (a) and (b) are relative permittivity and conductivity for hemorrhagic stroke, respectively. (c) and (d) are relative permittivity and conductivity for ischemic stroke, respectively.

TABLE 2. The SSIM and NRMSE for reconstructed images of phantom number 04 section 220 with ischemic stroke and 30dB SNR.

Methods	SSIM		NRMSE	
	permittivity	conductivity	permittivity	conductivity
BIM-Tikh	0.3960	0.3140	0.1589	0.4363
BIM-GenTikh	0.5315	0.4225	0.1350	0.3674
DBIM-Tikh	0.4159	0.3413	0.1541	0.3776
DBIM-GenTikh	0.5352	0.4544	0.1244	0.3433

TABLE 3. The SSIM and NRMSE for reconstructed images of phantom number 04 section 220 with hemorrhagic stroke and 20dB SNR.

Methods	SSIM		NRMSE	
	permittivity	conductivity	permittivity	conductivity
BIM-Tikh	0.3863	0.3077	0.1922	0.4801
BIM-GenTikh	0.5071	0.3700	0.1659	0.4365
DBIM-Tikh	0.4094	0.3362	0.1617	0.3893
DBIM-GenTikh	0.5093	0.4366	0.1366	0.3589

TABLE 4. The SSIM and NRMSE for reconstructed images of phantom number 04 section 220 with ischemic stroke and 20dB SNR.

Methods	SSIM		NRMSE	
	permittivity	conductivity	permittivity	conductivity
BIM-Tikh	0.3883	0.3038	0.1720	0.4554
BIM-GenTikh	0.5287	0.4037	0.1459	0.3962
DBIM-Tikh	0.4225	0.3189	0.1635	0.3995
DBIM-GenTikh	0.5351	0.4254	0.1310	0.3616

error (NRMSE) are computed and their values are reported in Tables 1 - 4. The NRMSE for relative permittivity and conductivity is obtained by (25).

$$NRMSE = \sqrt{\frac{\sum_{i=1}^{M} \left(x^r(r_i) - x^e(r_i)\right)^2}{\sum_{i=1}^{M} x^e(r_i)^2}} \tag{25}$$

In Eq. (25), x^r and x^e are the reconstructed and the exact values, respectively and M is the number of image pixels.

As seen in Figs. 2 and 3 and Tables 1 - 4, the proposed approach leads to the better quality for the reconstructed images and hence an improvement in the stroke classification.

V. CONCLUSION

Identifying the type of brain stroke is a realistic and vital issue. Microwave imaging techniques that are affordable and portable are one of the newest techniques for diagnosis. In this paper, we propose a new approach to reconstruct brain images using generalized Tikhonov regularization. This approach composed of three step. First using BIM with Tikhonov regularization method, the brain image is reconstructed. In the second step we choose a reference image by comparing the reconstructed image in the previous step with a MRI-based brain images set using SSIM criterion. At the last step we reconstruct the brain image by DBIM or BIM with generalized Tikhonov regularization method and the reference image. For verification, this approach is applied for two different SNRs 20dB and 30dB. The reconstructed images are depicted and the results are compared with original profile by two criteria: NRMSE and SSIM. SSIM and NRMSE, for relative permittivity and conductivity have improved at least 0.1 and about 0.03, respectively. This comparison shows the reconstructed images have better quality and accuracy.

REFERENCES

[1] P. M. Meyers, H. C. Schumacher, E. S. Connolly, E. J. Heyer, W. A. Gray, and R. T. Higashida, "Current status of endovascular stroke treatment," *Circulation*, vol. 123, no. 22, pp. 2591–2601, Jun. 2011.
[2] M. Hopfer, R. Planas, A. Hamidipour, T. Henriksson, and S. Semenov, "Electromagnetic tomography for detection, differentiation, and monitoring of brain stroke: A virtual data and human head phantom study," *IEEE Antennas Propag. Mag.*, vol. 59, no. 5, pp. 86–97, Oct. 2017.
[3] A. Fhager, S. Candefjord, M. Elam, and M. Persson, "Microwave diagnostics ahead: Saving time and the lives of trauma and stroke patients," *IEEE Microw. Mag.*, vol. 19, no. 3, pp. 78–90, May 2018.
[4] J. Liu, L. Chen, H. Xiong, and Y. Han, "Review of microwave imaging algorithms for stroke detection," *Med. Biol. Eng. Comput.*, May 2023, pp. 1–14.
[5] L. Guo, A. S. M. Alqadami, and A. Abbosh, "Stroke diagnosis using microwave techniques: Review of systems and algorithms," *IEEE J. Electromagn., RF Microw. Med. Biol.*, vol. 7, no. 2, pp. 122–135, Jun. 2022.
[6] V. Mariano, J. A. Tobon Vasquez, and F. Vipiana, "A novel discretization procedure in the CSI-FEM algorithm for brain stroke microwave imaging," *Sensors*, vol. 23, no. 1, p. 11, Dec. 2022.
[7] P. Lu and P. Kosmas, "Three-dimensional microwave head imaging with GPU-based FDTD and the DBIM method," *Sensors*, vol. 22, no. 7, p. 2691, Mar. 2022.
[8] P. Tournier, M. Bonazzoli, V. Dolean, F. Rapetti, F. Hecht, F. Nataf, I. Aliferis, I. El Kanfoud, C. Migliaccio, M. de Buhan, M. Darbas, S. Semenov, and C. Pichot, "Numerical modeling and high-speed parallel computing: New perspectives on tomographic microwave imaging for brain stroke detection and monitoring," *IEEE Antennas Propag. Mag.*, vol. 59, no. 5, pp. 98–110, Oct. 2017.
[9] I. Bisio, C. Estatico, A. Fedeli, F. Lavagetto, M. Pastorino, A. Randazzo, and A. Sciarrone, "Brain stroke microwave imaging by means of a newton-conjugate-gradient method in L^p Banach spaces," *IEEE Trans. Microw. Theory Techn.*, vol. 66, no. 8, pp. 3668–3682, Aug. 2018.
[10] I. Bisio, C. Estatico, A. Fedeli, F. Lavagetto, M. Pastorino, A. Randazzo, and A. Sciarrone, "Variable-exponent lebesgue-space inversion for brain stroke microwave imaging," *IEEE Trans. Microw. Theory Techn.*, vol. 68, no. 5, pp. 1882–1895, May 2020.
[11] D. W. Winters, B. D. Van Veen, and S. C. Hagness, "A sparsity regularization approach to the electromagnetic inverse scattering problem," *IEEE Trans. Antennas Propag.*, vol. 58, no. 1, pp. 145–154, Jan. 2010.
[12] C. Gilmore, P. Mojabi, and J. LoVetri, "Comparison of an enhanced distorted born iterative method and the multiplicative-regularized contrast source inversion method," *IEEE Trans. Antennas Propag.*, vol. 57, no. 8, pp. 2341–2351, Aug. 2009.
[13] X. Ye and X. Chen, "Subspace-based distorted-born iterative method for solving inverse scattering problems," *IEEE Trans. Antennas Propag.*, vol. 65, no. 12, pp. 7224–7232, Dec. 2017.
[14] P. Zhao, L. Liu, K. Xu, X. Ye, S. Chen, G. Wang, and C. H. Chan, "An improved subspace-regularized DBIM-MLGFIM method for three-dimensional inverse scattering problems," *IEEE Trans. Antennas Propag.*, vol. 69, no. 5, pp. 2798–2809, May 2021.
[15] Y. Zhong, M. Lambert, D. Lesselier, and X. Chen, "A new integral equation method to solve highly nonlinear inverse scattering problems," *IEEE Trans. Antennas Propag.*, vol. 64, no. 5, pp. 1788–1799, May 2016.
[16] K. Xu, Y. Zhong, and G. Wang, "A hybrid regularization technique for solving highly nonlinear inverse scattering problems," *IEEE Trans. Microw. Theory Techn.*, vol. 66, no. 1, pp. 11–21, Jan. 2018.
[17] N. Simonov, B. Kim, K. Lee, S. Jeon, and S. Son, "Advanced fast 3-D electromagnetic solver for microwave tomography imaging," *IEEE Trans. Med. Imag.*, vol. 36, no. 10, pp. 2160–2170, Oct. 2017.
[18] X. Chen, *Computational Methods for Electromagnetic Inverse Scattering*. Hoboken, NJ, USA: Wiley, 2018.
[19] Y. M. Wang and W. C. Chew, "An iterative solution of the two-dimensional electromagnetic inverse scattering problem," *Int. J. Imag. Syst. Technol.*, vol. 1, no. 1, pp. 100–108, 1989.
[20] W. C. Chew and Y. M. Wang, "Reconstruction of two-dimensional permittivity distribution using the distorted born iterative method," *IEEE Trans. Med. Imag.*, vol. 9, no. 2, pp. 218–225, Jun. 1990.
[21] Z. Wang, A. C. Bovik, H. R. Sheikh, and E. P. Simoncelli, "Image quality assessment: From error visibility to structural similarity," *IEEE Trans. Image Process.*, vol. 13, no. 4, pp. 600–612, Apr. 2004.
[22] B. Aubert-Broche, M. Griffin, G. B. Pike, A. C. Evans, and D. L. Collins, "Twenty new digital brain phantoms for creation of validation image data bases," *IEEE Trans. Med. Imag.*, vol. 25, no. 11, pp. 1410–1416, Nov. 2006.
[23] B. Aubert-Broche, A. C. Evans, and L. Collins, "A new improved version of the realistic digital brain phantom," *NeuroImage*, vol. 32, no. 1, pp. 138–145, Aug. 2006.
[24] C. Gabriel, "Compilation of the dielectric properties of body tissues at RF and microwave frequencies," Dept. Phys., King's Coll London, London, U.K., Tech. Rep. 0704-0188, 1996.

SAYYED SALEH SAYYED MOUSAVI was born in Mashhad, Iran, in March 1991. He received the B.S. and M.S. degrees in electrical engineering from the Ferdowsi University of Mashhad, Mashhad, Iran, in 2013 and 2016, respectively, where he is currently pursuing the Ph.D. degree. His research interests include transformation optic and microwave imaging.

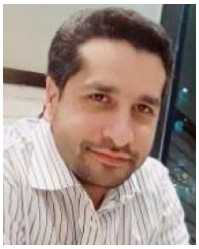

MOHAMMAD SAEED MAJEDI was born in Shiraz, Iran, in May 1983. He received the B.S. degree in electrical engineering from the Ferdowsi University of Mashhad, Mashhad, Iran, in 2006, the M.S. degree in electrical engineering from the Sharif University of Technology, Tehran, Iran, in 2008, and the Ph.D. degree in electrical engineering from the Ferdowsi University of Mashhad. In 2013, he joined the Department of Electrical Engineering, Ferdowsi University of Mashhad, where he is currently an Associate Professor. His research interests include antenna, microwave circuit, and microwave imaging.